Using radiative transfer equation to model absorption by thin Cu(In,Ga)Se2 solar cells with Lambertian back reflector

Nir Dahan, Zacharie Jehl, Jean Francois Guillemoles, Daniel Lincot, Negar Naghavi, Jean-Jacques Greffet

Using radiative transfer equation to model absorption by thin Cu(In,Ga)Se_2 solar cells with Lambertian back reflector

N. Dahan,[1,2,*] **Z. Jehl,**[2] **J. F. Guillemoles,**[2] **D. Lincot,**[2] **N. Naghavi,**[2] **and J.-J. Greffet**[1]

[1]*Laboratoire Charles Fabry, Institut d'Optique, CNRS - Université Paris-Sud, Campus Polytechnique, RD128, 91127 Palaiseau Cedex, France*
[2]*Institut de Recherche et Développement sur l'Energie Photovoltaïque, IRDEP (EDF/CNRS/Chimie-ParisTechUMR7174), 6 quai Watier, 78401 Chatou, France*
** nir_dahan@yahoo.com*

Abstract: We investigate the optical absorption in a thin Cu(In,Ga)Se_2 solar cell with a Lambertian white paint beneath a transparent back contact. Although this configuration has been proposed more than 30 years ago, it turns out that rigorous simulation of Maxwell's equations demand powerful numerical calculations. This type of approach is time consuming and does not provide a physical insight in the absorption mechanisms. Here, we use the radiative transfer equation to deal with multiple scattering of the diffuse part of the light. The collimated part is treated accounting for wave effects. Our model is in good agreement with optical measurements.

OCIS codes: (350.6050) Solar energy; (040.5350) Photovoltaic; (030.5620) Radiative transfer.

References and links

1. P. Jackson, D. Hariskos, E. Lotter, S. Paetel, R. Wuerz, R. Menner, W. Wischmann, and M. Powalla, "New world record efficiency for Cu(In,Ga)Se_2 thin film solar cells beyond 20%," Prog. Photovolt: Res. Appl. **19**, 894–897 (2011).
2. K. Orgassa, H. W. Schock, and J. H. Werner, "Alternative back contact materials for thin film Cu(In,Ga)Se_2 solar cells," Thin Solid Films **431**–**432**, 387–391 (2003).
3. A. Čampa, J. Krč, J. Malmström, M. Edoff, F. Smole, and M. Topič, "The potential of textured front ZnO and flat TCO/metal back contact to improve optical absorption in thin Cu(In,Ga)Se_2 solar cells," Thin Solid Films **515**, 5968–5972 (2007).
4. Z. Jehl Li Kao, N. Naghavi, F. Erfurth, J. F. Guillemoles, I. Gérard, A. Etcheberry, J. L. Pelouard, S. Collin, G. Voorwinden, and D. Lincot, "Towards ultrathin copper indium gallium diselenide solar cells: proof of concept study by chemical etching and gold back contact engineering," Prog. Photovolt: Res. Appl. **20**, 582–587 (2012).
5. E. Yablonovitch, "Statistical ray optics," J. Opt. Soc. Am. **72**, 899–907 (1982).
6. H. W. Deckman, C. R. Wronski, H. Witzke, and E. Yablonovitch, "Optically enhanced amorphous silicon solar cells," Appl. Phys. Lett. **42**, 968–970 (1983).
7. J. Morris, R. R. Arya, J. G. O'Dowd, and S. Wiedeman, "Absorption enhancement in hydrogenated amorphous silicon-based solar cells," J. Appl. Phys. **67**, 1079–1087 (1990).
8. M. A. Green, "Lambertian light trapping in textured solar cells and light-emitting diodes: analytical solutions," Prog. Photovolt: Res. Appl. **10**, 235–241 (2002).
9. J. Malmström, O. Lundberg, and L. Stolt, "Potential for light trapping in Cu(In,Ga)Se_2 solar cells," in *3rd World Conference on Photovoltaic Energy Conversion*, K. Kurokawa ed. (Arisumi, Osaka, Japan, 2003), pp. 344–347.
10. F. Leblanc, J. Perrin, and J. Schmitt, "Numerical modeling of the optical properties of hydrogenated amorphous-silicon-based p-i-n solar cells deposited on rough transparent conducting oxide substrates," J. Appl. Phys. **75**, 1074–1087 (1994).

#178436 - $15.00 USD Received 22 Oct 2012; revised 11 Dec 2012; accepted 3 Jan 2013; published 28 Jan 2013

11. M. Zeman, R. A. C. M. M. van Swaaij, J. W. Metselaar, and R. E. I. Schropp, "Optical modeling of a-Si:H solar cells with rough interfaces: effect of back contact and interface roughness," J. Appl. Phys. **88**, 6436–6443 (2000).
12. J. Krč, M. Zeman, F. Smole, and M. Topič, "Optical modeling of a-Si:H solar cells deposited on textured glass/SnO_2 substrates," J. Appl. Phys. **92**, 749–755 (2002).
13. J. Krč, M. Topič, M. Vukadinović, and F. Smole, "Optical modeling of a-Si:H-based solar cells with smooth and rough boundaries," in *16th European Photovoltaic Solar Energy Conference*, James & James ed. (Alden, Glasgow, UK, 2000), pp. 522–525.
14. J. Krč, F. Smole, and M. Topič, "Analysis of light scattering in amorphous Si:H solar cells by a one-dimensional semi-coherent optical model," Prog. Photovolt: Res. Appl. **11**, 15–26 (2003).
15. J. Springer, A. Poruba, A. Fejfar, M. Vanecek, L. Feitcknecht, N. Wyrsch, J. Meier, and A. Shah, "Nanotextured thin film silicon solar cells: optical model," in *16th European Photovoltaic Solar Energy Conference*, James & James ed. (Alden, Glasgow, UK, 2000), pp. 434–437.
16. J. Springer, A. Poruba, and M. Vanecek, "Improved three-dimensional optical model for thin-film silicon solar cells," J. Appl. Phys. **96**, 5329–5337 (2004).
17. R. Santbergen and R. J. C. van Zolingen, "The absorption factor of crystalline silicon PV cells: a numerical and experimental study," Sol. Energ. Mat. Sol. Cells **92**, 432–444 (2008).
18. G. E. Thomas and K. Stamnes, *Radiative Transfer in the Atmosphere and Ocean* (Cambridge, New York, 1999).
19. M. I. Mishchenko, L. D. Travis, and A. A. Lacis, *Multiple Scattering of Light by Particles: Radiative Transfer and Coherent Backscattering* (Cambridge, UK, 2006).
20. I. R. Howell, R. Siegel, and M. P. Mengüç, *Thermal Radiation and Heat Transfer* (CRC, Boca Raton, Florida, 2010).
21. A. K. Fung, *Microwave Scattering and Emission Models and Their Applications* (Artech House, Norwood, Mass., 1994).
22. L. Tsang, J. A. Kong, and K.-H. Ding, *Scattering of Electromagnetic Waves: Theories and Applications* (Wiley, New York, 2000).
23. M. S. Patterson, B. Chance, and B. C. Wilson, "Time resolved reflectance and transmittance for the non-invasive measurement of tissue optical properties," Appl. Opt. **28**, 2331–2336 (1989).
24. B. Lipovšek, J. Krč, O. Isabella, M. Zeman, and M. Topič, "Modeling and optimization of white paint back reectors for thin-lm silicon solar cells," J. Appl. Phys. **108**, 103115 (2010).
25. L. Ryzhik, G. Papanicolaou, and J. B. Keller, "Transport equations for elastic and other waves in random media," Wave Motion **24**, 327–370 (1996).
26. L. Roux, P. Mareschal, Nicolas Vukadinovic, J.-B. Thibaud, and J.-J. Greffet, "Scattering by a slab containing randomly located cylinders: comparison between radiative transfer and electromagnetic simulation," J. Opt. Soc. Am. A **18**, 374–384 (2001).
27. F. Ghmari, T. Ghbara, M. Laroche, R. Carminati, and J.-J. Greffet, "Influence of microroughness on emissivity," J. Appl. Phys. **96**, 2656–2664 (2004).
28. K. Tang, R. A. Dimenna, and R. O. Buckius, "Regions of validity of the geometric optics approximation for angular scattering from very rough surfaces," Int. J. Heat Mass Transfer **40**, 49–59 (1996).
29. R. Carminati and J.-J. Greffet, "Near-field effects in spatial coherence of thermal sources," Phys. Rev. Lett. **82**, 1660–1663 (1999).
30. C. F. Bohren and D. R. Huffman, *Absorption and Scattering of Light by Small Particles* (John Wiley & Sons, New York, 1983).
31. K. F. Evans and G. L. Stephens, "A new polarized atmospheric radiative transfer model," J. Quant. Spectrosc. Radiat. Transfer **46**, 413–423 (1991).
32. A. Ishimaru, *Wave Propagation and Scattering in Random Media* (Academic, New York, 1978).
33. P. Yeh, *Optical Waves in Layered Media* (Wiley, New-York, 1988).
34. M. A. Dupertuis, B. Acklin, and M. Proctor, "Generalized energy balance and reciprocity relations for thin-film optics," J. Opt. Soc. Am. A **11**, 1167–1174 (1994).
35. W. Szabelak and W. Nasalski, "Enhancement of cross-polarized beam components at a metamaterial surface," Appl. Phys. B **103**, 369–375 (2011).
36. P. C. Y. Chang, J. G. Walker, and K. I. Hopcraft, "Ray tracing in absorbing media," J. Quant. Spectrosc. Radiat. Transfer **96**, 327–341 (2005).
37. M. Bouttemy, P. Tran-Van, I. Gérard, T. Hildebrandt, A. Causier, J. L. Pelouard, G. Dagher, Z. Jehl, N. Naghavi, G. Voorwinden, B. Dimmler, M. Powalla, J. F. Guillemoles, D. Lincot, and A. Etcheberrya, "Thinning of CIGS solar cells: part I: chemical processing in acidic bromine solutions," Thin Solid Films **519**, 7207–7211 (2011).
38. P. J. Rostan, J. Mattheis, G. Bilger, U. Rau, and J. H. Werner, "Formation of transparent and ohmic ZnO:Al/$MoSe_2$ contacts for bifacial Cu(In,Ga)Se_2 solar cells and tandem structures," Thin Solid Films **480**–**481**, 67–70 (2005).
39. N. Dahan, Z. Jehl, T. Hildebrandt, J.-J. Greffet, J.-F. Guillemoles, D. Lincot, and N. Naghavi, "Optical approaches to improve the photocurrent generation in Cu(In,Ga)Se_2 solar cells with absorber thicknesses down to 0.5 μm," J. Appl. Phys. **112**, 094902 (2012).
40. J. Rousset, E. Saucedo, and D. Lincot, "Extrinsic doping of electrodeposited zinc oxide films by chlorine for

#178436 - $15.00 USD Received 22 Oct 2012; revised 11 Dec 2012; accepted 3 Jan 2013; published 28 Jan 2013

transparent conductive oxide applications," Chem. Mater. **21**, 534–540 (2009).
41. S. Kumar, A. Majumdar, and C. L. Tien, "The differential-discrete-ordinate method for solutions of the equation of radiative transfer," J. Heat Transfer **112**, 424–429 (1990).
42. Z. Jin and K. Stamnes, "Radiative transfer in nonuniformly refracting layered media: atmosphere-ocean system," Appl. Opt. **33**, 431–442 (1994).
43. J. Caron, C. Andraud, and J. Lafait, "Radiative transfer calculations in multilayer systems with smooth or rough interfaces," J. Mod. Opt. **51**, 575–595 (2004).
44. L. Li, "Bremmer series, R-matrix propagation algorithm, and numerical modeling of diffraction gratings," J. Opt. Soc. Am. A **11**, 2829–2836 (1994).

1. Introduction

Copper indium gallium diselenide (CIGS) is one of the most promising thin film solar cell technologies [1]. While increasing the development of commercial modules the issue of materials resources arises. Currently, indium is widely used in the production of flat screens found in computer and electronic devices. A continued growing demand over many years may result in a lack of indium. Therefore, reducing the amount of indium by thinning the absorber layer in solar cells is of main interest. The typical thickness of CIGS in commercial cells is about 2–2.5 μm. For this thickness, most of the light in the visible range is absorbed in a single pass due to the high absorption coefficient. In a thin film with a thickness on the order of 0.5 μm or less, the thickness of the absorber layer is smaller than the absorption depth of light; therefore, optical management is of crucial importance. With current technology, reducing the thickness of CIGS results in increased parasitic losses in the Mo back contact. Hence, it was proposed to replace the back contact by a more reflective material such as silver or gold [2–4].

While the previous discussion has been focussed on CIGS photovoltaic cells, the issue of enhancing absorption by thin cells is relevant for all materials. It is well known that scattering light in the absorber layer enhance the absorption in the cell by light trapping effect [5]. Since the refractive index of semi-conductors is high, the absorption near its bandgap energy can be enhanced significantly by trapping rays by total internal reflection. While this mechanism is well understood in the ray optics regime for a slab with one or two rough interfaces [5–9], modeling the scattering due to rough surfaces within the entire solar cell is much more complicated [10–17]. Of course, exact solutions of Maxwell's equations can always be calculated for a given cell configuration. However, this type of approach requires brute force numerical simulations, is time consuming, and does not provide a physical insight in the absorption mechanisms. It is thus desirable to explore the potential of alternative models. In the model proposed by Leblanc et al., the incident wave on a rough surface was divided into specular and diffuse components [10]. The specular light was assumed to be proportional to the Fresnel's coefficients such that energy is conserved and the angular distribution of the diffuse reflection and transmission were derived experimentally. Both absorption due to specular and diffuse light were calculated by the transfer matrix method but, without correlation between them. Zeman and Krč regarded the specular light as coherent and the diffuse light as incoherent treated with one-dimensional ray tracing [11–15]. The rough surfaces were assumed to be Lambertian or any angular distribution. Springer et al. used similar approach where they followed the diffuse light by Monte-Carlo technique [16, 17]. In the work of Santbergen and Zolingen, a net-radiation method was implemented to study the optical absorption of thick wafers ($> 300\,\mu$m) [17]. This is an incoherent energy transport equation which is not adequate for thin film solar cells.

An alternative approach is based on using the radiative transfer equation (RTE) which is a transport equation for diffuse intensity in scattering and absorbing media. This approach is very well developed in the context of atmospheric sciences [18, 19], mechanical engineering for radiative heat transport [20], microwave remote sensing [21, 22] or propagation in tissues [23]. Although the techniques for solving the RTE are well-known, their application to modeling ab-

#178436 - $15.00 USD Received 22 Oct 2012; revised 11 Dec 2012; accepted 3 Jan 2013; published 28 Jan 2013

sorption in thin solar cells raises a number of specific questions. First of all, a typical cell consists in several interfaces where specular reflection takes place. For structures with thicknesses on the order of the wavelength, interference effects cannot be neglected. It is thus necessary to account for interferences for the collimated part of the light whereas an incoherent model can be used for the diffuse component. When interferences are produced in an absorbing medium, a specific difficulty appears due to the fact that absorption is a non linear process. The standard implementation of RTE deals with losses in situations where the absorption length is much larger than the system size which is itself much larger than the wavelength (ray optics approximation). These media are known as semitransparent media. In the context of thin photovoltaic cells, both the system size and the absorption length are on the order of the wavelength. Another specific issue is the critical importance of properly dealing with total internal reflection at interfaces between lossy media with different refractive indices. In contrast with what happens for non lossy media, the transmission factor is non zero between lossy media for angles beyond the critical angle. In this context, accounting for the frustrated total internal reflection between lossy media plays a significant role. Hence, at first glance, thin solar cells appear not to be in the domain of validity of RTE. To our knowledge, it has not been used in solar cells applications [24].

In this paper, we revisit the question of using the radiative transfer equation for modeling absorption by a thin cell. It is usually considered that RTE can be used for systems where geometric optics is valid and the media can be considered to be semi transparent. While these conditions are sufficient conditions for RTE to be valid, they are not necessary. It turns out that RTE is not a purely phenomenological model. It can be derived from wave equations [19, 25]. Also, it is well known that the collimated part of the field is coherent whereas the diffuse part of the field is incoherent [19,22,25]. It is thus worth revisiting the question of its application to thin solar cells. The key question of the validity of RTE for wavelength scale layered systems has been addressed previously. A comparison between full electromagnetic numerical simulations and RTE equation has shown that the diffuse part of the energy is properly described by RTE [26]. RTE is equivalent to a ray tracing technique. The potential of ray tracing techniques to deal with absorption by rough surfaces has also been explored and it was found that they can model correctly absorption for both periodic [27] and random [28] surfaces with transverse length scales approaching the wavelength provided that there are no surface waves excitations. The origin of the failure of incoherent models when exciting surface waves is well understood: surface waves produce coherent fields along the interfaces [29]. For a stratified medium such as a solar cell, waves guided in large index layers could play a role similar to surface waves and therefore introduce long range coherence. However, as guiding layers are designed to be lossy, they are expected to vanish over distances on the order of the wavelength so that no long range coherence is expected. Hence, encouraged by these results, we apply the RTE to photovoltaic cells. In this work, we present a formalism where the collimated part of the light is treated using a coherent model accounting for interferences between the layers. The diffuse part of the light is modeled using the RTE. Scattering is included by introducing the bidirectional scattering distribution function of the interfaces. The multiple scattering is included by using the formalism of scattering matrix [18].

Our model is compared with experimental results. A proof of concept solar cell was realized with transparent conductive oxide (TCO) as a back contact (ZnO:Al) and white-paint on the rear interface to scatter the light back into the cell. Optical measurements show increased absorption by the cell in the infrared region due to the Lambertian reflection of the white paint. We report experimental results which are in good agreement with the model for an absorbing layer of 400 nm.

The paper is organized as follows. The next section describes the optical model within the

#178436 - $15.00 USD Received 22 Oct 2012; revised 11 Dec 2012; accepted 3 Jan 2013; published 28 Jan 2013

semi-coherent approach. In section 3, calculations by the model are compared with experiment results. Discussion on the model and further calculations of the short circuit current for solar cells with different back-contacts are given in section 4. Finally, conclusions are summarized in section 5. A detailed presentation of the numerical technique to solve the semi-coherent RTE is given in Appendix A.

2. Description of the optical model

The goal of this section is to introduce the general formalism of RTE from the perspective of the matrix approach [18]. We briefly introduce the definition of the key quantities and show how they can be used to derive the absorption in the cell.

2.1. Basic formalism

The basic quantity used in radiative transfer theory is the specific intensity $I(z,\hat{\mathbf{u}})$ which is the radiative power per unit area and unit solid angle in direction $\hat{\mathbf{u}}$ at depth z. The flux through an area dA in direction $\hat{\mathbf{u}}$ in a solid angle dΩ is given by:

$$\mathrm{d}F = I(z,\hat{\mathbf{u}})\cos\theta\ \mathrm{d}\Omega. \tag{1}$$

Note that this quantity is scalar so that we are neglecting polarization. In principle, one could use the vectorial RTE which contains all the information on polarization using the Stokes vector [30, 31]. However, solar light is unpolarized and scattering by white paint depolarizes the light. Hence, we will be working in the scalar approximation hereafter. We will be introducing different layers located at $z = l_m$. It is convenient to analyze separately the energy propagating upwards and downwards. The flux integrated over all upward and downward directions is thus:

$$F^{\pm}(l_m) = \int_{\pm 2\pi} I_d^{\pm}(l_m;\hat{\mathbf{u}})\cos\theta\ \mathrm{d}\Omega. \tag{2}$$

The net flux at an interface is then given by $F(l_m) = F^+(l_m) - F^-(l_m)$ and the absorption in a volume between layers at l_m and l_n with $l_m > l_n$ is given by:

$$A_d = \frac{F(l_n) - F(l_m)}{F_{\mathrm{inc}}}, \tag{3}$$

where F_{inc} is the incident flux. In summary, once the specific intensities are known in the system, it is easy to derive the absorption in a given layer. We now turn to the equations that govern the radiative energy transport.

2.2. Interface scattering

The formalism is particularly useful to deal with multiple scattering at different interfaces. The key ingredient to account for scattering is the transmission and reflection at an interface. In the field of optics and radiometry, this quantity is known as bidirectional scattering distribution function (BSDF) such that $R_d(\hat{\mathbf{u}},\hat{\mathbf{u}}')$ is the BRDF and $T_d(\hat{\mathbf{u}},\hat{\mathbf{u}}')$ is the BTDF. They relate the incident intensity in direction $\hat{\mathbf{u}}' = (\theta',\phi')$ to the scattered intensity into direction $\hat{\mathbf{u}} = (\theta,\phi)$. In our context, it is useful to introduce explicitly the splitting between the specular and the diffuse components of the BSDF:

$$\begin{aligned} R_d(\hat{\mathbf{u}},\hat{\mathbf{u}}') &= R_{d0}(\hat{\mathbf{u}},\hat{\mathbf{u}}')\delta(\hat{\mathbf{u}}-\hat{\mathbf{u}}') + R_{dd}(\hat{\mathbf{u}},\hat{\mathbf{u}}') \\ T_d(\hat{\mathbf{u}},\hat{\mathbf{u}}') &= T_{d0}(\hat{\mathbf{u}},\hat{\mathbf{u}}')\delta(\hat{\mathbf{u}}-\hat{\mathbf{u}}_t) + T_{dd}(\hat{\mathbf{u}},\hat{\mathbf{u}}') \end{aligned} \tag{4}$$

where the subscript $d0$ represents the specular component of the diffuse light, δ is the Dirac delta function, and $\hat{\mathbf{u}}_t$ is related to $\hat{\mathbf{u}}'$ by Snell's law. The subscript dd represents the scattering

#178436 - $15.00 USD Received 22 Oct 2012; revised 11 Dec 2012; accepted 3 Jan 2013; published 28 Jan 2013

by the diffuse light – it is the contribution from diffuse light to diffuse light. In addition, there is also contribution of coherent light to the diffuse part. T_{cd} represents the fraction that is extinguished from the coherent beam in transmission and is scattered into diffuse. It is the same function (matrix, as we shall see later) like T_{dd}; but, we keep the subscript notation to remember its origin. In reflection, it is denoted by R_{cd}. A schematic description of each contribution to the diffuse light is illustrated in Fig. 1 where $(+)$ sign is defined in the illumination direction of the sunlight. Given these terms, the specific intensity emerging from an interface can be cast in the following form:

$$\begin{aligned}\frac{I_d^+(0_m,\hat{\mathbf{u}})}{n_m^2} &= \int_{+2\pi} T_d^+(\hat{\mathbf{u}},\hat{\mathbf{u}}')\frac{I_d^+(L_{m-1},\hat{\mathbf{u}}')}{n_{m-1}^2}\mu'\,\mathrm{d}\Omega' + \\ &\quad \int_{-2\pi} R_d^-(\hat{\mathbf{u}},\hat{\mathbf{u}}')\frac{I_d^-(0_m,\hat{\mathbf{u}}')}{n_m^2}\mu'\,\mathrm{d}\Omega' + \\ &\quad T_{cd}^+(\hat{\mathbf{u}},\hat{\mathbf{u}}')I_c^+(L_{m-1},\hat{\mathbf{u}}') + R_{cd}^-(\hat{\mathbf{u}},\hat{\mathbf{u}}')I_c^-(0_m,\hat{\mathbf{u}}') \qquad (5)\end{aligned}$$

where L_m is the thickness of layer m, $\mu = \cos\theta$, and $d\Omega = \sin\theta\,\mathrm{d}\theta\,\mathrm{d}\phi$.

With these definitions, it can be understood that accounting for multiple scattering amounts to include the multiple reflections between different interfaces. The procedure is explained in detail in Appendix A. Here, we want to examine in some detail some effects which need to be taken into account when dealing with interfaces separating media with different refractive index so that reflection and total internal reflection may take place.

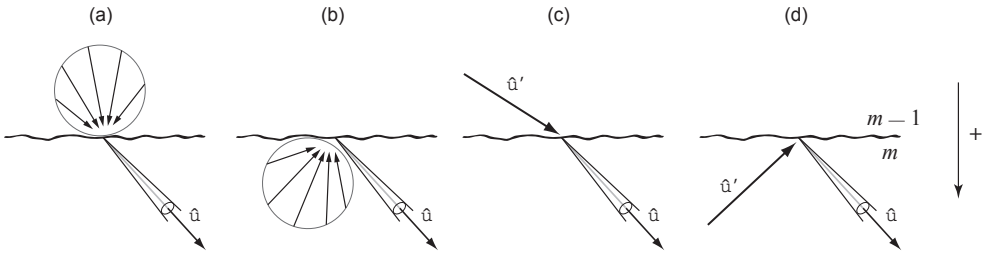

Fig. 1. Schematic description of interface scattering between layers $m-1$ and m. The diffuse intensity emerging from the surface can be due to four contributions: (a) transmission from diffuse light, T_d^+; (b) reflection from diffuse light, R_d^-; (c) transmission from collimated light, T_{cd}^+; and (d) reflection from collimated light, R_{cd}^-.

2.3. Coherent and incoherent specific intensity

We first discuss the importance of coherence of the field. When dealing with absorbing systems with a thickness much larger than the wavelength, interferences can be neglected because after averaging over all angles and all frequencies, the interference effects vanish. Here, we want to emphasize that when dealing with the absorption of the collimated component of the incident field, there is no averaging. If in addition, the thickness of the system is smaller than the wavelength, then the resulting absorption will depend significantly on whether the absorbing layer is located at a maximum or a minimum of the field. This is due to the well known Fabry-Perot oscillations. With this picture in mind, the coherent effects must be taken into account when computing the absorption of the collimated incident beam. Conversely, when dealing with the diffuse component of the incident light, interferences can be neglected because scattering by a random medium introduces random phases. For our purpose, we need to split the specific intensity in two parts: the collimated which is coherent and the diffuse which is incoherent [22, 32].

#178436 - $15.00 USD Received 22 Oct 2012; revised 11 Dec 2012; accepted 3 Jan 2013; published 28 Jan 2013

The collimated part is treated as a plane wave impinging on a multilayer system. The electromagnetic fields through the cell are found using the transfer matrix method [33]. It is an exact solution of Maxwell's equations that takes into account interference effects and multiple reflections within the different layers. The second part is the diffuse light which originates from scattering processes in the cell, such as rough surface, particles, etc. The transport of the diffuse light in the cell is modeled using the RTE, taking into account multiple scattering.

2.4. *Absorption of coherent light*

Here, we want to stress that absorption is a nonlinear phenomenon. Indeed, the local dissipation rate is proportional to the square of the electric field. This property results in an interference term appearing when writing the energy conservation at an interface. The intuitive relation of using the Fresnel's factors as

$$R_F + T_F = 1 \tag{6}$$

is no longer valid. Instead, one finds:

$$R_F + T_F = 1 + \mathscr{M}; \qquad \mathscr{M} = 2\frac{\mathrm{Im}(Q_i)}{\mathrm{Re}(Q_i)}\mathrm{Im}(r), \tag{7}$$

where Q_i corresponds to the perpendicular component of the wave vector in the medium of the incident wave and r is the reflection coefficient, as defined in Appendix B. The additional term in the right side of Eq. (7), $\mathscr{M}$, is known as the mixed Poynting vector [10, 34–36]. It stems from interference between the incident wave and the reflected wave in the absorbing media. Nevertheless, it can be neglected provided that $\mathrm{Im}(n)/\mathrm{Re}(n) < 0.1$ [34]. In order to quantify the $\mathscr{M}$ term in our cell, we calculate it for CIGS/ZnO:Al and CIGS/CdS interface, as a function of incident wavelength and direction. The results are shown in Fig. 2. Large values are obtained for wavelengths below 1μm and at large incident angles. However, since in isotropic scattering the intensity decays according to the cosine's law, the energy at angles above 60° is small. In addition, we will show later that since the light is scattered by the white paint into the ZnO:Al layer, the energy in the CIGS layer is null beyond the critical angle hence the large $\mathscr{M}$ there is meaningless, and therefore it will be ignored hereafter.

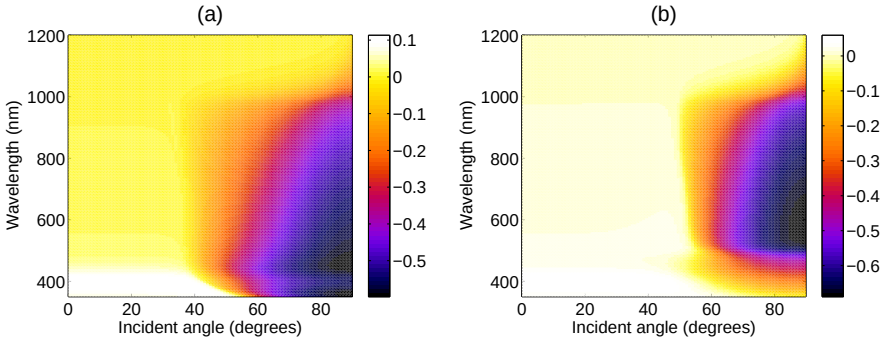

Fig. 2. The mixed Poynting's vector term ($\mathscr{M}$) as a function of wavelength and incident angle when unpolarized light illuminates from CIGS in case of: (a) CIGS - ZnO:Al and (b) CIGS - CdS interface.

2.5. *Leaky transmission*

Another interesting phenomenon which did not receive much attention in the literature is leaky transmission. When a plane wave illuminates a flat interface from medium 1 to medium 2 at

#178436 - $15.00 USD Received 22 Oct 2012; revised 11 Dec 2012; accepted 3 Jan 2013; published 28 Jan 2013

angles beyond the critical angle, part of the light may be transmitted if medium 2 has losses. This effect is obtained directly from Fresnel's coefficients for both polarizations. Note that in this case the transmission does not follow Snell's law. The direction of energy flow is found from the Poynting's vector by $\cos\theta_t = \mathbf{S}\cdot\hat{\mathbf{z}}/|\mathbf{S}|$. An example of transmission values from dielectric to lossy material is given in Fig. 3. This leaking energy has a fundamental consequence in optical management of solar cells. As the active layer is lossy and is bounded between semiconductor and metal or two semiconductors that are also lossy, light *is not* totally reflected even though it is beyond the critical angle. Indeed, $k_{z,2}$ has a real part when n_2 is complex indicating propagation in medium 2. In other words, light is not fully trapped in the active layer, as it is often assumed to be. As noted above, the transmission on a flat interface does not follow Snell's law so that $n_1^2\,\mu_1\,d\Omega_1 \neq n_2^2\,\mu_2\,d\Omega_2$. Instead, the energy conservation gives

$$\frac{I_t^+(0_2,\hat{\mathbf{u}})}{I_{\text{inc}}^+(L_1,\hat{\mathbf{u}}')} = T_F(\hat{\mathbf{u}},\hat{\mathbf{u}}')\,\frac{\mu_1\,\mathrm{d}\Omega_1}{\mu_2\,\mathrm{d}\Omega_2} \tag{8}$$

where $I_t^+(0_2,\hat{\mathbf{u}})$ is the transmitted intensity in medium 2.

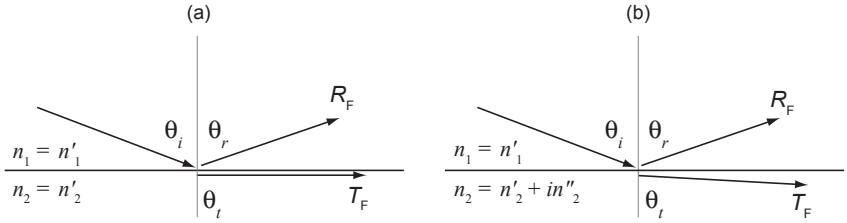

Fig. 3. Transmission from medium 1 at $\theta_i = 60^\circ$ to medium 2 where $n_1 = 2$ and $n_2 = 1.5 + in_2''$. (a) $n_2'' = 0$: $R_F = 1$ and $T_F = 0$ at $\theta_t = 90^\circ$. (b) $n_2'' = 0.1$: $R_F = 0.6864$ and $T_F = 0.3136$ at $\theta_t = 84.4^\circ$.

3. Experimental results

In this section, we compare experimental measurements and calculations of light absorption by a solar cell structure with transparent back contact and white paint. A proof of concept solar cell structure was realized using the following process. A standard CIGS film on Mo substrate is etched down to 1000 nm thickness from the front side in the bromine solution, as described in Ref. [37]. The standard solar cell stack (CdS / i:ZnO / ZnO:Al) is then deposited on the absorber, and an encapsulation is performed [4]. After the lift-off of the structure, a back side etching of the CIGS is performed down to a final thickness of 400 nm. In a realistic configuration, a TCO is needed between the absorber and the white paint for charge carrier extraction. We have deposited a 200 nm ZnO:Al spacer layer at the back side of the CIGS by sputtering. The ohmic contacts between CIGS and ZnO:Al were investigated by Rostan et al. and are not considered in this work [38].

At this stage, the cell is semi-transparent and all the interfaces are flat. We have measured the reflection and transmission from the cell using a UV/visible/IR spectrometer (Perkin-Elmer λ–900, spectral resolution: 10 nm) using an integrating sphere. From these measurements, it is possible to find the absorption in the cell by $A = 1 - R - T$. We compare the measurement with calculation in Fig. 4(a), curve (A). As can be seen, there is a good agreement with the model (coherent light only) indicating that we use the correct thicknesses and refractive index of the

#178436 - $15.00 USD Received 22 Oct 2012; revised 11 Dec 2012; accepted 3 Jan 2013; published 28 Jan 2013

different layers (for example, at 1μm wavelength the refractive indices are: $n_{\text{glass}} = 1.514 + i3.16 \times 10^{-6}$; $n_{\text{ZnO:Al}} = 1.543 + i1.97 \times 10^{-2}$; $n_{\text{i:ZnO}} = 2.005$; $n_{\text{CdS}} = 2.270 + i1.16 \times 10^{-2}$; $n_{\text{CIGS}} = 3.001 + i5.39 \times 10^{-2}$; and $n_{\text{IMM}} = 1.5$). The high absorption in the IR spectra is due to the free-carriers in the ZnO:Al layers.

After this first characterization, a white paint (Spectralon) is attached mechanically on the rear side of the ZnO:Al such that an air gap is assumed to be between them. The reflection of the white paint was taken in the simulations as isotropic (Lambertian) with total reflectivity of 99% in the given spectral range. Since no light is transmitted from the cell the absorption in this configuration is given by $A = 1 - R$. We then perform the same spectroscopic characterizations, and compare with simulation results [curve (B) in Fig. 4(a)]. It is clearly seen that the absorption in the long wavelengths, near the bandgap of CIGS (1.15eV), are due to the white paint as a back reflector as well as enhanced absorption by the free carriers in ZnO:Al layers.

In curve (C), we compare the absorption by the cell when the white paint is adhered to the TCO using index matching medium (IMM). Its refractive index is $n_{\text{IMM}} = 1.5$ which is close to that of ZnO:Al in the IR spectra, and is assumed to be constant. A schematic illustration of

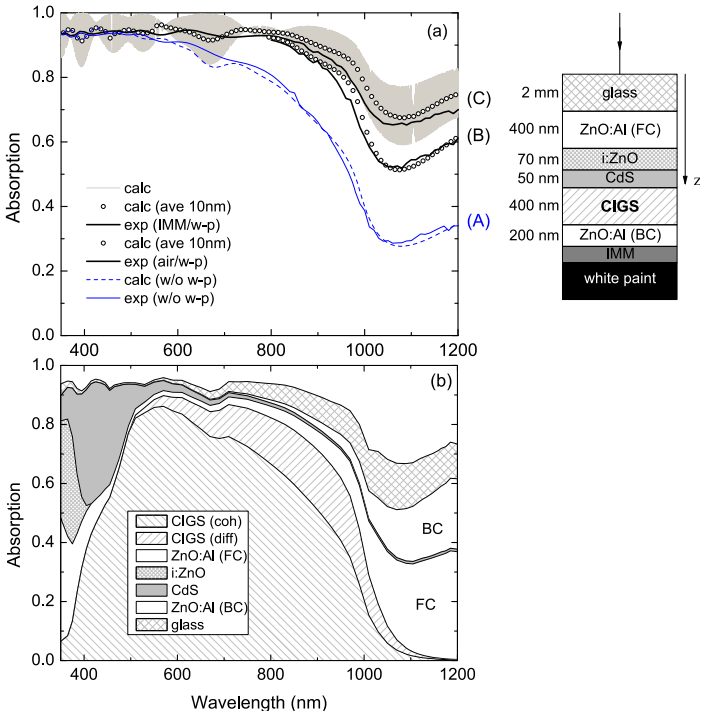

Fig. 4. (a) Spectral absorption by a CIGS solar cell as depicted in the inset. Curve (A) denotes measurement (solid) and calculation (dash) of solar cell without white paint (w-p) beneath the back contact ($A = 1 - R - T$). Curve (B) indicates measurement (solid) and calculation (dots) when the w-p is attached to the back contact with air gap between them ($A = 1 - R$). Curve (C) is when the w-p is adhered to the back contact using index matching media (IMM). Dense oscillations are obtained due to the thick glass superstrate (gray line). Numerical averaged is performed over a spectral window of 10 nm (dots), as the resolution of the spectrometer (for all the curves). (b) Spectral absorption in the different layers. For clarity, in the CIGS layer we show the absorbed light by the coherent and the diffuse parts. 'FC' ('BC') stands for the ZnO:Al in the front (back) contact.

#178436 - $15.00 USD Received 22 Oct 2012; revised 11 Dec 2012; accepted 3 Jan 2013; published 28 Jan 2013

the cell is shown in the inset of Fig. 4. The simulation is given in gray line to show the dense oscillations coming from Fabry-Perot interference in the thick glass. Then, we averaged this calculation with the same spectral resolution as the spectrometer (10 nm) to retrieve the smooth behavior (dots) of the experiment. It should be noted that this procedure was performed also for curves (A) and (B).

4. Discussion and simulations

Based on the good agreement between the experimental results and calculations, we can predict the absorption in the different layers. In particular, the absorption in the absorber layer which is proportional to the quantum efficiency and the short circuit current.

The results are shown in Fig. 4(b). In the light absorption of CIGS we discern between coherent absorption due to the collimated sunlight, and diffuse absorption due to the diffuse light originated from scattering on the white paint. For 400 nm thickness of CIGS, the diffuse light affects the absorption at wavelength larger than 500 nm. Its maximum is in the IR (800 – 1000 nm wavelength). At longer wavelengths, the absorption in ZnO:Al becomes dominant. Furthermore, it is seen that the buffer layer absorbs substantially in the visible range. As we have reported elsewhere [39], this absorption can be avoided by replacing the CdS with ZnS. Since the ZnS is a semi-conductor with a higher energy bandgap (3.6 eV) than the CdS (2.4 eV), more light will transmit into the CIGS layer and will be absorbed there. The high absorption in the ZnO:Al should also be reduced. Replacing it by a more transparent oxide, e.g. ZnO:Cl, can reduce its absorption in the IR and in the UV spectra [40].

The enhanced absorption by the cell in the presence of the white paint can be understood by the propagation of light in the cell. It is described schematically in Fig. 5. Collimated sunlight impinges on the cell and undergoes reflections and transmissions on the flat interfaces until it reaches the Lambertian back reflector (white paint). After it reaches the white paint, all the collimated light is reflected isotropically in the layer above (n_2). This diffuse light propagates upward in the cell such that in layers with larger refractive index, e.g. at $n_3 > n_2$, light beyond the critical angle equals zero (zone III). At layers with smaller refractive index (n_1), total reflection occurs beyond the critical angle such that light is trapped in the cell (zone II). It means, that the confinement of light depends on the refractive index of the medium close to the white paint (n_2 in Fig. 5). Back to the results of Fig. 4(a), curve (B) corresponds to a structure where there is an air gap between the white paint and the back contact ($n_2 = n_1$); therefore, no light is trapped in the cell. Regarding curve (C), there is IMM between the white paint and the solar cell

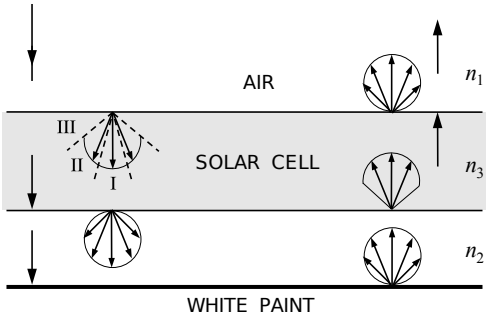

Fig. 5. Schematic description of light trapping effect. Assuming $n_3 > n_2 > n_1$, zone I, II, III corresponds to light cone in n_1, n_2, and n_3, respectively. Therefore, the intensity in zone III equals zero, and on the interface from solar-cell to air, light in zone II is totally reflected.

#178436 - $15.00 USD Received 22 Oct 2012; revised 11 Dec 2012; accepted 3 Jan 2013; published 28 Jan 2013

($n_2 = n_{\mathrm{IMM}}$). Hence, the light trapping is only in zone II, which is according to the refractive index of the IMM.

In Fig. 6(a), we display the absorption in all the layers of a more realistic solar cell structure, i.e., the white paint is mounted on the back contact directly – without IMM. In addition, to avoid the absorption in the thick glass, an antireflection layer (MgF_2, 100 nm thick) is used. Consequently, the total absorption by the cell is very similar to the one obtained in Fig. 4(b). When examining how the absorption is distributed within the layers, we find the absorption in the CIGS is slightly larger.

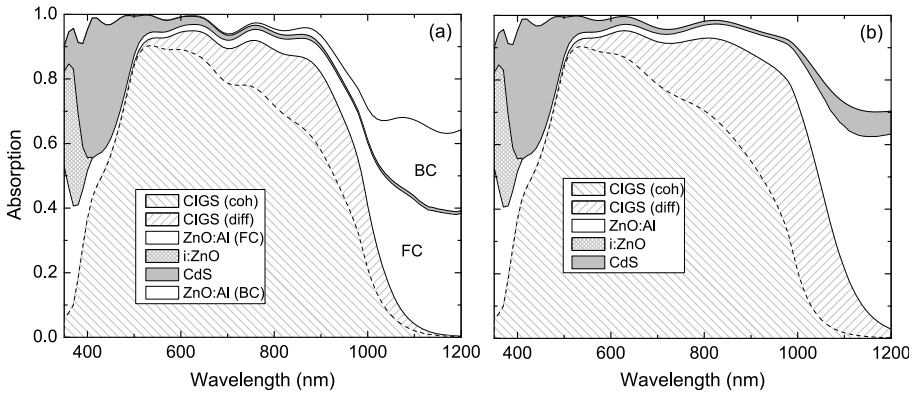

Fig. 6. Spectral absorption in the different layers of the CIGS solar cell described in Fig. 4, with an antireflection layer (MgF_2 – 100 nm thickness) instead of the glass superstrate, and (a) without IMM layer. (b) Without IMM layer and the back contact itself reflects the light as a white paint. As a result, the diffuse light in the CIGS layer is isotropic.

From the preceding analysis, it is clear that the absorption in CIGS layer could be even larger, if the back contact would reflect as a white paint. Calculations of this hypothetical cell are shown in Fig. 6(b). The absorption due to the coherent light is almost not changed whereas the contribution of the diffuse light to absorption is increased dramatically. Note that the absorption edge is shifted toward the IR region. This effect can be manifested in the short circuit current, calculated by

$$\mathrm{J_{sc}} = q \int A_\lambda (m_{\mathrm{CIGS}}) I_{\mathrm{solar}}(\lambda) \frac{\lambda}{hc} d\lambda \tag{9}$$

where q is the elementary charge, $A_\lambda(m_{\mathrm{CIGS}})$ is the spectral absorption in the CIGS layer [given by Eq. (34)], hc/λ is the energy per wavelength, and I_{solar} is the sunlight (AM1.5). Comparison of $\mathrm{J_{sc}}$ for different back contacts as a function of CIGS thickness is shown in Fig. 7. It is seen that Mo is equivalent to ZnO:Al. Gold is known to enhance the reflection relative to Mo and also has good ohmic contact [4]. However, it is not suitable for mass production due to its high cost. White paint beneath the ZnO:Al layer is much less expensive and give similar results for CIGS thickness above 500 nm and slightly better results for thinner absorber. A cell with back contact that reflects as white paint is anticipated to improve significantly the $\mathrm{J_{sc}}$, e.g., 30 mA/cm^2 at 100 nm CIGS thickness compare to 15 mA/cm^2 for Mo with flat interface. It is worth mentioning that the results of the $\mathrm{J_{sc}}$ are based only on optical modeling. A realistic model for thin films should include also electrical effects on the interface, and possible chemical modifications of the interface.

#178436 - $15.00 USD Received 22 Oct 2012; revised 11 Dec 2012; accepted 3 Jan 2013; published 28 Jan 2013

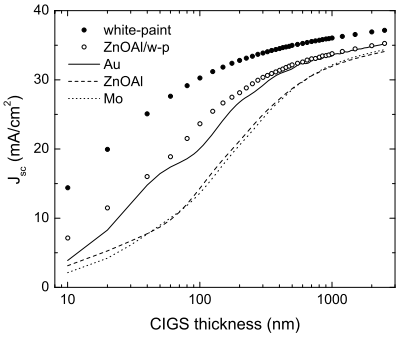

Fig. 7. Calculated short circuit current as a function of CIGS thickness for different back contacts.

5. Conclusions

We have investigated theoretically and experimentally the light absorption in a CIGS based solar cell with TCO back contact and white paint reflector. Enhanced absorption in the cell was obtained near the CIGS bandgap, resulting from light trapping in its high refractive index. Further absorption was calculated in the IR spectra when the TCO itself reflects as white paint, i.e., all the incident light is reflected isotropically. This enhancement is beyond what can be achieved with a flat gold or silver mirror. Simulated short circuit current are more than double as compared to the standard Mo back contact, at very thin layers. In the theoretical part, we have introduced in detail a two-dimensional semi-coherent model. The collimated sunlight and its specular components are analyzed using the transfer matrix method where the diffuse part of the light is treated using the RTE. The main limitations of our model are due to the mixed Poynting vector. Also, in case of metallic layers supporting surface plasmons or transparent high index layers supporting long range guided modes, coherent effects not accounted by the model will be significant. In our investigated cell, the white paint reflects as Lambertian surface. It provides the simplest model for surface scattering that satisfies energy conservation and reciprocity. Although the assumptions of the RTE are based on ray optics, which presume scale length much larger than the wavelength, we have found it to agree well in wavelength scale structure. This enables the use of the model in various stratified media with irregular interfaces in which interference effects are important. It includes different types of solar cells, thermophotovoltaics, photodetectors and light emitting devices.

A. Radiative transfer equation in stratified media

In this Appendix, we aim to give a detail derivation of the model presented in the paper. Although a large part can be found in the literature, it is distributed among different disciplines. Moreover, it is not formulated as proposed here: to incorporate calculations of electromagnetic fields (in the collimated part) with energy transport calculations (in the diffuse light). We begin with the quadrature rule which is a discretization of the polar angles along with the corresponding weights to each angle. The boundary conditions on an irregular interface are introduced in section A.2. Finally, a mathematical framework how to calculate the absorption in a given layer using the RTE is presented in section A.3.

#178436 - $15.00 USD Received 22 Oct 2012; revised 11 Dec 2012; accepted 3 Jan 2013; published 28 Jan 2013

A.1. *Quadrature rule in stratified media*

In a stratified media, it is of crucial importance to define the polar angles in each layer appropriately in order to consider the change in the refractive index between two adjacent layers. Assuming a flat interface separating two different media. In the high index medium there are two regions: below and beyond the critical angle. Moreover, in a multi-layer structure one needs to pay attention to the case where a layer with high refractive index is placed between two different layers with lower refractive indices. In this case, the critical angles with respect to both materials should be considered. This issue has been discussed by numerous articles [41–43]. The procedure we use to find the polar angles is similar to the one discussed by Caron et at. [43]. First, we sort the layers in ascending order according to their real part of refractive index such that the first layer has the lowest refractive index. The layers in the sorted structure are denoted by $j = 1, 2, ..., J$ and its size can be smaller than that of the investigated structure if the same material is used. In the first layer, we set even angles and corresponding weights according to double Gaussian quadrature in the range $\mu = \cos\theta \in [0, 1]$. In the second layer, the refractive index is larger hence in the region below the critical angle, θ_c, we set the angles according to the Snell's law,

$$\mu_2 = \sqrt{1 - \left(\frac{n_1}{n_2}\right)^2 (1 - \mu_1^2)} \tag{10}$$

with the corresponding weights [18],

$$w_2 = \left(\frac{n_1}{n_2}\right)^2 \left(\frac{\mu_1}{\mu_2}\right) w_1, \tag{11}$$

where we recall that only the real part of the refractive index is used to determine the angles. In the region beyond the critical angle, i.e. $\mu \in [0, \mu_c]$, we set the angles and weights according to double Gaussian quadrature. These sets of angles and weights is used to determine the quadrature in the next layer in the region below the critical angle. For directions beyond the critical angle, the double Gauss method is used. The same procedure is continued until the layer with the largest refractive index.

The number of angles (known also as streams), N, in each layer is proportional to the refractive index of the layer n. In layer j,

$$N(j) = N_0 n_j. \tag{12}$$

where N_0 is the number of angles in the first layer. From this arrangement, the number of streams in each layer can be written also as

$$N(j) = N(j-1) + N'(j) \tag{13}$$

where $N'(j)$ is the number of streams in layer j beyond the critical angle. A careful study shows that for a given structure N_0 is not a free variable, if the critical angles between all the layers are to be accounted for. In fact, in a stratified media with different materials, one should consider a minimum number of even streams with respect to the materials that are used, i.e., at least two streams beyond the critical angle yields,

$$N_{0,\min} = \frac{2}{\Delta n_{\min}} \tag{14}$$

where $\Delta n_{\min}$ is the minimum difference between adjacent refractive indices in the sorted structure (or, smaller as we wish). For a given intensity, the integration over the polar angles is calculated using the double Gauss method such that

$$\int I(\mu)\mu \, \mathrm{d}\mu \approx \sum_j^N I(\mu_j)\, \mu_j w_j. \tag{15}$$

#178436 - $15.00 USD Received 22 Oct 2012; revised 11 Dec 2012; accepted 3 Jan 2013; published 28 Jan 2013

The integration over the azimuth angle, ϕ, is usually performed when expanding the azimuthal dependence of the scattering function in a Fourier series [18]. Herein, where we use only flat and Lambertian interfaces, the scattering function is independent on ϕ; hence,

$$F = \iint I(\mu,\phi)\,\mu\,\mathrm{d}\mu\,\mathrm{d}\phi = 2\pi\int I(\mu)\,\mu\,\mathrm{d}\mu. \tag{16}$$

A.2. Boundary conditions on a single interface

The specific intensity emerging from an interface is given in section 2.2, Eq. (5). We emphasize that since only collimated light can contribute to diffuse light, these terms have the same meaning as sources in the RTE, as can be seen by the last two terms in Eq. (5). In a flat interface, for instance, they are equal to zero and therefore do not contribute to diffuse light. In the same manner, we write the diffuse intensity in the opposite direction,

$$\begin{aligned}\frac{I_d^-(L_{m-1},\hat{\mathbf{u}})}{n_{m-1}^2} &= \int_{-2\pi} T_d^-(\hat{\mathbf{u}},\hat{\mathbf{u}}')\frac{I_d^-(0_m,\hat{\mathbf{u}}')}{n_m^2}\mu' d\Omega' + \\ &\int_{+2\pi} R_d^+(\hat{\mathbf{u}},\hat{\mathbf{u}}')\frac{I_d^+(L_{m-1},\hat{\mathbf{u}}')}{n_{m-1}^2}\mu' d\Omega' + \\ &T_{cd}^-(\hat{\mathbf{u}},\hat{\mathbf{u}}')I_c^-(0_m,\hat{\mathbf{u}}') + R_{cd}^+(\hat{\mathbf{u}},\hat{\mathbf{u}}')I_c^+(L_{m-1},\hat{\mathbf{u}}').\end{aligned} \tag{17}$$

Let us also include propagation in layer m to distance l_m. In case the medium absorbs, the intensity will be attenuated according to Beer's law along the ray, i.e.,

$$I_d(l_m,\hat{\mathbf{u}}) = I_d(0_m,\hat{\mathbf{u}})\exp(-\tau_m/\mu) \tag{18}$$

where $\tau_m = 2k_0\mathrm{Im}(n_m)l_m$. Thus, the intensities on an interface including propagation in layer m are,

$$\begin{aligned}\frac{I_d^+(l_m,\hat{\mathbf{u}})}{n_m^2} &= e^{-\tau_m/\mu}\int_{+2\pi} T_d^+(\hat{\mathbf{u}},\hat{\mathbf{u}}')\frac{I_d^+(L_{m-1},\hat{\mathbf{u}}')}{n_{m-1}^2}\mu' d\Omega' + \\ &e^{-\tau_m/\mu}\int_{-2\pi} R_d^-(\hat{\mathbf{u}},\hat{\mathbf{u}}')\frac{I_d^-(l_m,\hat{\mathbf{u}}')}{n_m^2}e^{-\tau_m/\mu'}\mu' d\Omega' + \\ &e^{-\tau_m/\mu}\left[T_{cd}^+(\hat{\mathbf{u}},\hat{\mathbf{u}}')I_c^+(L_{m-1},\hat{\mathbf{u}}') + R_{cd}^-(\hat{\mathbf{u}},\hat{\mathbf{u}}')I_c^-(0_m,\hat{\mathbf{u}}')\right]\end{aligned} \tag{19}$$

and,

$$\begin{aligned}\frac{I_d^-(L_{m-1},\hat{\mathbf{u}})}{n_{m-1}^2} &= \int_{-2\pi} T_d^-(\hat{\mathbf{u}},\hat{\mathbf{u}}')\frac{I_d^-(l_m,\hat{\mathbf{u}}')}{n_m^2}e^{-\tau_m/\mu'}\mu' d\Omega' + \\ &\int_{+2\pi} R_d^+(\hat{\mathbf{u}},\hat{\mathbf{u}}')\frac{I_d^+(L_{m-1},\hat{\mathbf{u}}')}{n_{m-1}^2}\mu' d\Omega' + \\ &T_{cd}^-(\hat{\mathbf{u}},\hat{\mathbf{u}}')I_c^-(0_m,\hat{\mathbf{u}}') + R_{cd}^+(\hat{\mathbf{u}},\hat{\mathbf{u}}')I_c^+(L_{m-1},\hat{\mathbf{u}}').\end{aligned} \tag{20}$$

We write the equations above, (19) and (20), in a matrix formalism,

$$\begin{pmatrix} I_d^+(m) \\ I_d^-(m-1)\end{pmatrix} = \begin{bmatrix} T_d^+(m-1,m) & R_d^-(m-1,m) \\ R_d^+(m-1,m) & T_d^-(m-1,m)\end{bmatrix}\begin{pmatrix} I_d^+(m-1) \\ I^-(m)\end{pmatrix} + \begin{pmatrix} C^+(m-1,m) \\ C^-(m-1,m)\end{pmatrix} \tag{21}$$

such that each term can be understood. We omit the angles for brevity and keep only the layers in the notation where $(m-1,m)$ relates between the interface at the end of layer $m-1$ (L_{m-1}) and the interface at a distance l_m in layer m. The matrix given in Eq. (21) is called the scattering matrix between layers m and $m-1$, denoted by $\tilde{\mathbf{S}}(m-1,m)$. We recall that the $C^{\pm}$ terms corresponds to the source of the equation, stems from the collimated light.

#178436 - $15.00 USD Received 22 Oct 2012; revised 11 Dec 2012; accepted 3 Jan 2013; published 28 Jan 2013

A.2.1. Collimated light

The computation of the collimated light has two objectives. The first, is to know how much of the coherent light is absorbed by a specific layer. This is calculated by the Poynting's vector flux on the boundaries of the layer

$$A_c(m) = \frac{[\mathbf{S}(0_m) - \mathbf{S}(L_m)] \cdot \hat{\mathbf{z}}}{\mathbf{S}_{\text{inc}} \cdot \hat{\mathbf{z}}} \tag{22}$$

where $\mathbf{S}(l_m)$ and $\mathbf{S}_{\text{inc}}$ are the Poynting's vector at distance l in layer m and of the incident wave, respectively. The second aim is to find the intensities of the collimated light on the interfaces, I_c, in order to use it as a source term in the RTE. They are related to the Poynting's vector by the flux, where

$$F^{\pm} = \mathbf{S}^{\pm} \cdot \hat{\mathbf{z}} = \left|\mathbf{S}^{\pm}\right| \cos\theta, \tag{23}$$

and, on the other hand,

$$F^{\pm} = \int_{\pm 2\pi} I_c^{\pm}(\hat{\mathbf{u}}')\delta(\hat{\mathbf{u}} - \hat{\mathbf{u}}')\mu' \mathrm{d}\Omega' = I_c^{\pm}(\hat{\mathbf{u}})\cos\theta. \tag{24}$$

Thus, $I_c = |\mathbf{S}|$.

A.2.2. Diffuse light

As pointed out by Eq. (4), the scattering of the diffuse light contains two terms: the specular part and the diffuse part. In general, each of them should be found according to the specific interface. Here, we examine only two types of interfaces: flat and Lambertian.

On a flat interface, only the specular part exist and the diffuse part equal to zero. The reflection and transmission factors are given by Fresnel's factors for plane waves whereas for intensities one needs to consider the deviation in the angular beam within the change of n^2. For example, on an interface between layers 1 and 2, the relations between the intensities and the Fresnel's factors are given by [18]

$$\begin{aligned} R_{d0}^{+}(\hat{\mathbf{u}}, \hat{\mathbf{u}}) &= \frac{I_d^{-}(L_1, \hat{\mathbf{u}})/n_1^2}{I_d^{+}(L_1, \hat{\mathbf{u}})/n_1^2} = \frac{I_d^{-}(L_1, \hat{\mathbf{u}})}{I_d^{+}(L_1, \hat{\mathbf{u}})} = R_F(\hat{\mathbf{u}}, \hat{\mathbf{u}}) \\ T_{d0}^{+}(\hat{\mathbf{u}}, \hat{\mathbf{u}}') &= \frac{I_d^{+}(0_2, \hat{\mathbf{u}})/n_2^2}{I_d^{+}(L_1, \hat{\mathbf{u}}')/n_1^2} = \frac{I_d^{+}(0_2, \hat{\mathbf{u}})}{I_d^{+}(L_1, \hat{\mathbf{u}}')} \left(\frac{n_1}{n_2}\right)^2 = T_F(\hat{\mathbf{u}}, \hat{\mathbf{u}}'). \end{aligned} \tag{25}$$

In order to have light beyond the critical angle, a scattering process is necessary either by rough surface, gratings, or particles. The simplest model for surface scattering is the Lambertian interface which scatter all the impinging light isotropically. Therefore, the specular reflection/transmission is fully suppressed ($R_{d0} = T_{d0} = 0$) and the diffuse reflection/transmission [i.e., $R_{dd}(\hat{\mathbf{u}}, \hat{\mathbf{u}}')$ or $T_{dd}(\hat{\mathbf{u}}, \hat{\mathbf{u}}')$ in Eq. (4)] is constant – regardless of incident and emerging directions. White paint is known to reflect the incident light isotropically with a high BRDF of $R_d^{+} = 0.99/\pi$.

A.3. Solution of the RTE

So far, we have found the scattering matrix between two adjacent layers, given in Eq. (21). The same equation can be written to relate between the first layer and layer m,

$$\begin{pmatrix} I_d^{+}(m) \\ I_d^{-}(0) \end{pmatrix} = \begin{bmatrix} T_d^{+}(0,m) & R_d^{-}(0,m) \\ R_d^{+}(0,m) & T_d^{-}(0,m) \end{bmatrix} \begin{pmatrix} I_d^{+}(0) \\ I_d^{-}(m) \end{pmatrix} + \begin{pmatrix} C^{+}(0,m) \\ C^{-}(0,m) \end{pmatrix}. \tag{26}$$

#178436 - $15.00 USD Received 22 Oct 2012; revised 11 Dec 2012; accepted 3 Jan 2013; published 28 Jan 2013

where the geometry of the stratified structure with the corresponding notation is shown in Fig. 8. In order to find the scattering matrix herein, we use the recursive relation. After a little algebra, one set of equations yield,

$$\begin{aligned}
T^+(0,m) &= T^+(m-1,m)\,Q^+(0,m)\,T^+(0,m-1)\\
R^-(0,m) &= R^-(m-1,m)+T^+(m-1,m)\,Q^+(0,m)\,R^-(0,m-1)\,T^-(m-1,m)\\
C^+(0,m) &= C^+(m-1,m)+T^+(m-1,m)\,Q^+(0,m)\times\\
&\quad \left[C^+(0,m-1)+R^-(0,m-1)\,C^-(m-1,m)\right]\\
Q^+(0,m) &= \{\mathbb{1}-R^-(0,m-1)\,R^+(m-1,m)\}^{-1}
\end{aligned} \tag{27}$$

and another set of equations give

$$\begin{aligned}
T^-(0,m) &= T^-(0,m-1)\,Q^-(0,m)\,T^-(m-1,m)\\
R^+(0,m) &= R^+(0,m-1)+T^-(0,m-1)\,Q^-(0,m)\,R^+(m-1,m)\,T^+(0,m-1)\\
C^-(0,m) &= C^-(0,m-1)+T^-(0,m-1)\,Q^-(0,m)\times\\
&\quad \left[C^-(m-1,m)+R^+(m-1,m)\,C^+(0,m-1)\right]\\
Q^-(0,m) &= \{\mathbb{1}-R^+(m-1,m)\,R^-(0,m-1)\}^{-1}.
\end{aligned} \tag{28}$$

Although the two sets of relation seems to be the same, they are not completely identical. However, notice that they will be, if we replace $+$ with $-$, m with $m-1$, and $m-1$ with 0. The Q terms is the signature to the multiple reflection inside the structure, as was discussed in details by Li [44]. Let us emphasize that the order of multiplying the different variables will be very important in the matrix notation.

The initialization is straightforward in this notation. For any scattering variable, the initial condition is given by $R^{\pm}(0,1)$, $T^{\pm}(0,1)$, or $C^{\pm}(0,1)$ which is the interaction of light on the first

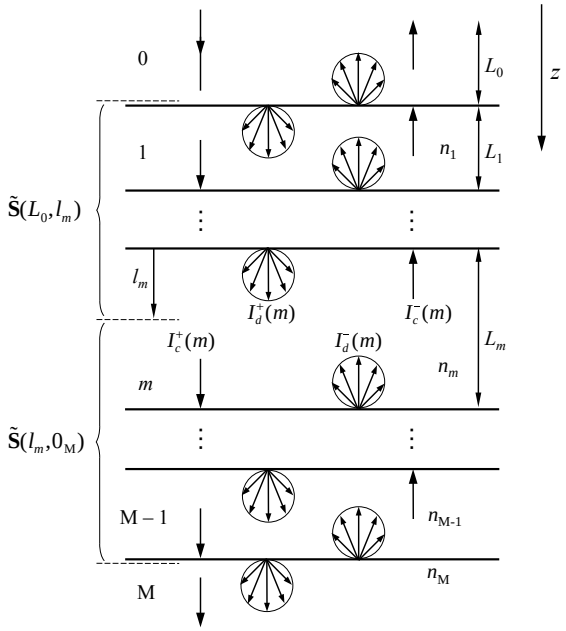

Fig. 8. Geometry of the system and schematic notation of the different variables.

#178436 - $15.00 USD Received 22 Oct 2012; revised 11 Dec 2012; accepted 3 Jan 2013; published 28 Jan 2013

interface only. For example, in case of flat interface, it will be simply the Fresnel's reflection and transmission coefficients. The contribution from the coherent part to the diffuse part will be, of course, zero.

In order to solve the RTE numerically, we used the regular discretization process. In the polar directions, the intensity in layer m can be written as a vector where each term corresponds to the intensity in different angle according to the quadrature rule introduced in section A.1

$$I(z;\hat{\mathbf{u}}) = \mathbf{I}(z;\hat{\mathbf{u}}_j) = \begin{pmatrix} I(z;\hat{\mathbf{u}}_1) \\ I(z;\hat{\mathbf{u}}_2) \\ \vdots \\ I(z;\hat{\mathbf{u}}_{N(m)}) \end{pmatrix}. \tag{29}$$

The reflection and transmission become matrices with different sizes according to the interface and direction of light. For example, consider an interface between layers $m-1$ and m. The transmission matrix $\mathbf{T}_d^+(m-1,m)$ needs to correlate between $N(m-1)$ streams of the incoming intensity to $N(m)$ streams of the outgoing intensity. Therefore, it is not a square matrix. It has a size of $N(m)\times N(m-1)$. With the same rationality, the transmission function in the opposite direction $\mathbf{T}_d^-(m-1,m)$ has a size of $N(m-1)\times N(m)$. The reflection matrices are square with a size according to the layer of the incoming light. Herein, $\mathbf{R}_d^+(m-1,m)$ stands for light coming from layer $m-1$ therefore its size is $N(m-1)\times N(m-1)$ and the size of $\mathbf{R}_d^-(m-1,m)$ is $N(m)\times N(m)$. Although each matrix has a different size, the scattering matrix in Eq. (21) becomes composition of the reflection and transmission matrices,

$$\tilde{\mathbf{S}}(m-1,m) = \begin{bmatrix} \mathbf{T}_d^+(m-1,m) & \mathbf{R}_d^-(m-1,m) \\ \mathbf{R}_d^+(m-1,m) & \mathbf{T}_d^-(m-1,m) \end{bmatrix} \tag{30}$$

with a size of $[N(m)+N(m-1)]\times[N(m-1)+N(m)]$ which is square. The source terms become vectors with a size according to the direction of light. $\mathbf{C}^+(m-1,m)$ describes the diffuse intensity in the $(+)$ direction, i.e., in layer m. Accordingly, it has a size of $N(m)\times 1$. For the same reason, $\mathbf{C}^-(m-1,m)$ has a size of $N(m-1)\times 1$. The same arguments hold when we calculate the scattering matrix and the intensities between any layers, e.g., 0 and m shown in Eq. (26) – but in a matrix form.

In order to calculate the absorption in a given layer in the stratified media, we need to know first the intensities in that layer. The intensity in a distance l in layer m can be found by solving Eq. (26) twice. Once, from the top of the first interface L_0, to the desired distance l_m.

$$\begin{pmatrix} \mathbf{I}_d^+(l_m;\hat{\mathbf{u}}_j) \\ \mathbf{I}_d^-(L_0;\hat{\mathbf{u}}_j) \end{pmatrix} = \tilde{\mathbf{S}}(L_0,l_m)\begin{pmatrix} \mathbf{I}_d^+(L_0;\hat{\mathbf{u}}_j) \\ \mathbf{I}_d^-(l_m;\hat{\mathbf{u}}_j) \end{pmatrix} + \begin{pmatrix} \mathbf{C}^+(L_0,l_m) \\ \mathbf{C}^-(L_0,l_m) \end{pmatrix}. \tag{31}$$

$\mathbf{I}_d^+(L_0;\hat{\mathbf{u}}_j)$ is the diffuse light incident on the cell. In our discussion, the light from Sun is fully coherent hence $\mathbf{I}_d^+(L_0;\hat{\mathbf{u}}_j)=0$. The second time we use the equation is between l_m and the end of the structure 0_M assuming no radiation illuminates the structure from the $(-)$ direction,

$$\begin{pmatrix} \mathbf{I}_d^+(0_M;\hat{\mathbf{u}}_j) \\ \mathbf{I}_d^-(l_m;\hat{\mathbf{u}}_j) \end{pmatrix} = \tilde{\mathbf{S}}(l_m,0_M)\begin{pmatrix} \mathbf{I}_d^+(l_m;\hat{\mathbf{u}}_j) \\ 0 \end{pmatrix} + \begin{pmatrix} \mathbf{C}^+(l_m,0_M) \\ \mathbf{C}^-(l_m,0_M) \end{pmatrix}. \tag{32}$$

Using the intensities at a given plane, the flux is derived by the following integration,

$$F^{\pm}(l_m) = 2\pi \sum_j^{N(m)} \mathbf{I}_d^+(l_m;\hat{\mathbf{u}}_j)\mu_j w_j \tag{33}$$

where the net flux is $F = F^+ - F^-$. Finally, the absorption is derived by the contribution from the diffuse part [Eq. (3)] and the collimated part [Eq. (22)] as,

$$A(m) = A_d(m) + A_c(m). \tag{34}$$

#178436 - $15.00 USD Received 22 Oct 2012; revised 11 Dec 2012; accepted 3 Jan 2013; published 28 Jan 2013

B. Definition of Fresnel's coefficients

In this section, we briefly define the Fresnel's coefficients for a flat interface for TE and TM polarizations. Assuming an interface in the *xy* plane separating medium 1 and 2 where $\hat{\mathbf{z}}$ is a unit vector normal to the interface, and n_j is the refractive index of medium j such that $\mathrm{Im}(n) \geq 0$. The wave vector in each medium is defined by

$$\mathbf{k}_j = (\mathbf{k}_\parallel, k_{z,j}) \tag{35}$$

where $\mathbf{k}_\parallel$ is the parallel wave vector in the *xy* plane, i.e., $\mathbf{k}_\parallel = (k_x, k_y)$ and is chosen to be real since it remains constant when the collimated light propagates in the cell, thus

$$k_\parallel = \mathrm{Re}(k_j) \sin\theta_j \tag{36}$$

where $k_j = n_j(\omega/c)$. The perpendicular component in the z direction is given by

$$k_{z,j} = \sqrt{k_j^2 - k_\parallel^2} \tag{37}$$

whose imaginary part is non-negative. Using these definitions, the Fresnel's coefficients for the fields are given by

$$r_{ij} = \frac{Q_i - Q_j}{Q_i + Q_j}\,, \qquad t_{ij} = \frac{2Q_i}{Q_i + Q_j} \tag{38}$$

where $Q_j = k_{z,j}$ for TE polarization, and $Q_j = k_{z,j}/n_j^2$ for TM polarization. The Fresnel's factors for the energy are derived by

$$R_F = \left|r_{ij}\right|^2\,, \qquad T_F = \frac{\mathrm{Re}(Q_j)}{\mathrm{Re}(Q_i)} \left|t_{ij}\right|^2. \tag{39}$$

Acknowledgments

This work is supported by the ANR's HABISOL program within the ULTRACIS Project and partially by the PVCiS Project.